

KARST DETECTION USING LOW-COST
ELECTRICAL RESISTIVITY METER

by
Benjamin D. Goffin

Thesis submitted to the faculty of the University of Virginia
in partial fulfillment of the requirements for the degree of

MASTER OF SCIENCE
In
Civil Engineering

May 2018

KARST DETECTION USING LOW-COST
ELECTRICAL RESISTIVITY METER

APPROVED BY:

Dr. Steven Chase
(Chairman)

Dr. Lindsay Ivey-Burden
(Thesis Director)

Dr. John Miller
(Research Professional)

DATE OF APPROVAL: 04/09/2018

ACKNOWLEDGMENT

Foremost, I would like to express my sincere gratitude to my academic advisor Prof. Lindsay Ivey-Burden for the trust she placed in me and the encouragement she offered throughout my studies.

I would also like to sincerely thank Prof. Steven Chase and Prof. John Miller for the expertise and the counseling they provided while serving on my defense committee.

My appreciation extends to all the staff, faculty and students of the University of Virginia who made my years on grounds worthwhile – including my friends Abdul and Charles, and my girlfriend Erin.

Last but not the least, I would like to recognize the families Goffin-Kettelle, Feuchtenberger, and Graff, for their loving support during my pursuit of the American Dream!

B.D.G.

ABSTRACT

About one-fifth of the United States is underlain by soluble rock and has the potential to develop voids within the subsurface (karst). It has been shown that property damages resulting from sinkhole formation in karst terrain amount to hundreds of millions of dollars each year. Different geophysical investigations (investigation methods that do not require any digging), are commonly employed to assess the potential risk of karst. However, most geophysical equipment from commercial vendors has very complex inner workings and costs tens of thousands of dollars. The present work extended the previous understanding on the fabrication of low-cost electrical resistivity (ER) meters and proposed the design of a new prototype to perform independent ground surveys. The developed device implemented inexpensive, user-friendly integrated circuit modules able to inject a current, measure the site's response, and characterize the local properties of soil and rock. The reliability of this ER meter was assessed using a series of test resistors. In this confirmatory test, the device proved to be accurate over a wide range of magnitudes. This ER meter also showed the potential for many practical applications. In a tabletop laboratory setting, the prototype successfully sounded overlying soil covers and correctly identified the lateral variations in apparent resistivity values along a transverse. The results from this study indicate that low-cost ER meters are capable of detecting underground discontinuities such as voids in an effort to prevent sinkhole formation in karst-prone areas.

Keywords: Geophysical testing, Electrical resistivity, VES, CST, Karst, Sinkholes

TABLE OF CONTENTS

AKNOWLEDGMENT	II
ABSTRACT	III
TABLE OF CONTENTS	IV
LIST OF FIGURES	V
LIST OF TABLES	VII
LIST OF ACRONYMS/ABBREVIATIONS.....	VIII
1. INTRODUCTION.....	1
2. LITERATURE REVIEW	2
2.1. KARST FORMATION AND SINKHOLE COLLAPSE	2
2.2. CURRENT STATE OF GEOPHYSICAL INVESTIGATION.....	3
2.3. THE BENEFITS OF ELECTRICAL RESISTIVITY METHODS.....	5
2.4. THE FABRICATION OF LOW-COST ER METER	7
3. DEVELOPING A LOW COST ER METER.....	8
3.1. DEVELOPMENT BOARDS.....	8
3.2. ANALOG INPUTS	9
3.2.1. <i>Ammeter</i>	9
3.2.2. <i>Voltmeter</i>	9
3.3. DIGITAL OUTPUTS.....	11
3.4. INTERFACING WITH MODULES.....	11
3.5. THE INEXPENSIVE COST OF THE DESIGN.....	13
3.6. THE RELIABILITY OF THE PROPOSED DEVICE.....	14
4. METHODOLOGY	18
4.1. ER THEORY	18
4.2. EXPERIMENT ONE	21
4.3. EXPERIMENT TWO.....	23
5. RESULTS AND DISCUSSION	25
5.1. EXPERIMENT ONE	25
5.2. EXPERIMENT TWO.....	29
6. LIMITATIONS.....	32
7. CONCLUSION	34
REFERENCES.....	35
APPENDIX	39

LIST OF FIGURES

Figure 1. Stages in the development of cover collapse sinkholes (adapted from Culshaw and Waltham, 1987)	2
Figure 2. Conventional resistivity analysis of the subsurface using electrodes uniformly spaced in a line according to Wenner array (adapted from Sharma, 1997).....	5
Figure 3. Arduino Uno development board consisting of microcontroller, USB port, digital pins, analog pins, barrel jack, voltage regulator, power supply, and ground	8
Figure 4. Inner workings of an analog voltmeter made up of a two-resistor voltage divider	9
Figure 5. Wiring of the proposed low-cost ER meter consisting of microcontroller, 9V battery, voltage divider, DC current sensor, LCD screen, I2C module, SD card module, DC power supply, and series of resistors under test.	12
Figure 6. Level of accuracy of the proposed device during confirmatory testing	15
Figure 7. Exponential relationship between variations in resistance readings and current levels as shown by the dashed line of robust linear fit $a=1.34$ and $b=-0.70$	16
Figure 8. Strong negative correlation between the variations in the resistance readings and the levels of current for the different values of resistance (Ohm). The shaded region represents the confidence interval of the correlation coefficient at 95%	17
Figure 9. Floodplain resistivity survey (values obtained from Herman, 2001)	20
Figure 10. Karst terrain underlain by weathered limestone bedrock reproduced in a tabletop laboratory setting	22
Figure 11. VES performed by progressively spreading the electrodes of a Wenner array in a tabletop setting	22
Figure 12. CST along a profile (dashed line) intercepting a void buried under 5 cm of soil	24
Figure 13. VESs of a test bed containing an artificial layer of fissured limestone between the depths of 12 and 21 cm	26
Figure 14. VES 1 indicating a potential limestone layer of apparent resistivity of 407 Ohm-m between 11 and 23 cm	27
Figure 15. VES 2 indicating a potential limestone layer of apparent resistivity of 512 Ohm-m between 8 and 21 cm.	27

Figure 16. High repeatability based on the strong positive correlation between the two VES datasets at the different effective depths (cm). The shaded region represents the confidence interval of the correlation coefficient at 95%.....	28
Figure 17. Parallel CSTs of a test bed containing a 10-cm-long artificial void intercepting two profiles at 20 cm.....	30
Figure 18. Spatial variation of apparent resistivity (Ohm-m) coinciding with the location of the artificial void in the test bed	30
Figure 19. Robust modeling by median polish of the spatial variation of apparent resistivity (Ohm-m). Disks' radius are proportional to the square root of the residuals.....	31

LIST OF TABLES

Table 1. Theoretical resistance across standard loads placed in parallel with a high-impedance voltmeter	11
Table 2. Cost breakdown of the proposed low-cost ER meter	13
Table 3. Results from confirmatory testing of the proposed ER meter against sets of known resistors	14
Table 4. Electrode array configuration (adapted from Samouëlian et al., 2005)	18
Table 5. Tabletop resistivity measurements of VES1-2.....	25
Table 6. Tabletop resistivity measurements of CST1-5.....	29

LIST OF ACRONYMS/ABBREVIATIONS

AC	Alternating Current
ADC	Analog-to-Digital Converter
CS	Chip Select
CST	Constant Separation Traversing
DC	Direct Current
ER	Electrical Resistivity
FWI	Full-Wave Inversion
GPR	Ground Penetrating Radar
IC	Integrated Circuit
I2C	Inter-Integrated Circuit
I/O	Input/Output
IDE	Integrated Development Environment
MAPE	Mean Absolute Percent Error
MASW	Multi-channel Analysis of Surface Waves
MISO	Master Input Slave Output
MOSI	Master Output Slave Input
RSD	Relative Standard Deviation
SCL	Serial Clock Line
SDA	Serial Data Line
SLK	Serial Clock
SP	Self-Potential
SPI	Serial Peripheral Interface
USCS	Unified Soil Classification System
VES	Vertical Electrical Sounding

1. INTRODUCTION

Found all across the United States, karst is a distinctive landscape formed by the dissolution of bedrock (Ford and Williams 1989). The erosion of karst terrain results in the presence of underlying voids, which are susceptible to form sinkholes.

Population growth and urban development have both stressed very sensitive karst systems. In recent years, the ground instability of these terrains has been a growing a concern. Sinkhole occurrences have increased at rates that are atypical of geological processes (Brinkmann, Parise and Dye 2007). In states like Florida, sinkhole claims tripled between 2006 and 2009, amounting to more than \$1.3 billion of property damage over the same period of time (Florida Senate Interim Report 104 2011).

While Gutierrez et al. still expect the amount of induced karst hazards to rise in the future (2014), gaining site-specific knowledge of karst systems may help prevent sinkhole collapse from occurring (Veni, et al. 2001). The use of certain noninvasive investigation methods such as electrical resistivity (ER) meters permit the detection of karstic cavities and conduits (Zhu, Currens and Dinger 2011; Farooq, et al. 2012; Land 2012). However, such commercial instruments represent a significant cost and have very complex inner workings.

Facing the same limitations, previous works (Becker, 2003; Mikailu et al. 2015; Juhari et al., 2017) proposed the design of different low-cost ER meters. Built upon those studies, this thesis aims to offer the design of an effective and affordable ER device that is easy to assemble and operate. The accuracy of such a device is studied, and its potential limitations are explored. Then, different tests are performed in tabletop laboratory setting to assess the applicability of the proposed ER meter to karst exploration.

2. LITERATURE REVIEW

In order to gain a better understanding of karst detection by a fabricated ER meter, this report first covers the subjects of karst formation and sinkhole collapse, the current state of geophysical investigation, the benefits of ER methods, and lastly the fabrication of a low-cost ER meter.

2.1. Karst formation and sinkhole collapse

This work is most concerned with solution depressions, interchangeably referred to as sinkholes and dolines. Even small sinkhole collapses can pose a serious threat to public safety and the integrity of infrastructures and transportation networks (Newton 1987). While the existence, location and extent of karstic features are difficult to determine, some commonalities of karstic features are known such as the underlying rock, soil cover, and aggravating factors.

Construction problems and catastrophic dropouts of sinkholes due to rock dissolution mainly involve limestone and dolostone. These rock formations are respectively composed of calcite (calcium carbonate) and dolomite (calcium-magnesium carbonate), both highly soluble in acidic water. Chemical weathering can alter a rock mass by enlarging its primary porosity at the grain level, as well as its secondary porosity in the form of fissures. However, erosion processes occur mainly at penetrable joints and bedding planes (White 1988).

Such solution pathways in the bedrock can draw downward the overlying zone of soft soil known as epikarst. In the case of subsidence sinkholes, a concave surface depression develops in the soil cover. Alternatively, when dealing with cover collapse sinkholes, a void forms beneath a soil arch. In the latter case, the raveling and further erosion enables the soil dome to expand until the roof reaches a critical thickness and collapses (figure 1).

Rock openings as small as 6 in. in diameter have been reported to generate domes 100 times wider (Sowers 1996). Cavities grow gradually but an increased infiltration rate at the ground surface or fluctuations in the

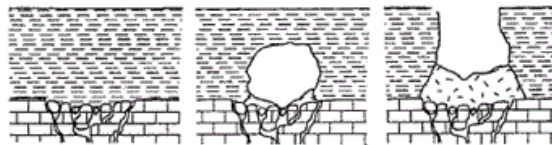


Figure 1. Stages in the development of cover collapse sinkholes (adapted from Culshaw and Waltham, 1987)

groundwater piezometric level can aggravate their expansion.

While common processes involved in karst formation have been identified, it is important to recognize their variability and understand the risk in extrapolating to generalities (Jennings 1985). Because each site is a unique response to multiple processes acting on the subsurface (Trudgill 1985), subsurface investigations play a crucial role in characterizing the local properties of soil and rock.

2.2. Current state of geophysical investigation

Traditionally, soil test borings have been used to explore conditions underground. However, in the context of karst assessment, Quinlan and Ewers (1985) compare this effort to throwing a dart at a map of the United States hoping to hit the Mississippi River. Geophysical methods are far more useful as they are sensitive to contrast in physical properties of soils over continuous coverage (Kaufmann, Deceuster and Quinif 2012).

Inherently, noninvasive geophysical methods help to quickly explore karst system and direct investigation efforts without requiring any digging. Before focusing on the ER survey, which is what was created as part of this study, some of the most common commercially available techniques will be briefly discussed as part of this work.

Ground Penetrating Radar (GPR) is a popular method for karst detection that is based on the weak attenuation of radar waves. Kruse et al. (2006) showed the effectiveness of 2D and 3D GPR scans for imaging both larger- and smaller-scale cavities and conduits. Because GPR scans are limited when the subsurface is electrically conductive, its customary use strongly depends on the absence of a clay soil cover or saturated zone at a specific site.

Seismic refraction is the one of three types of seismic investigations used in geophysical testing. It uses first-arrival signals to characterize media and resultantly often fails to define deeper material and neglects voids in the bedrock. Alternatively, the Multi-channel Analysis of Surface Waves (MASW) is based on the dispersion properties of surface waves and requires averaging properties of whole volumes of media for each frequency. At greater depths, the averages are such that embedded voids may be overlooked. The Full-Waveform Inversion (FWI) method overcomes the limitations of the refraction and MASW techniques by utilizing the entire seismic waveform. Both pressure- and shear-wave velocities are inverted independently and simultaneously for validation of profiles.

From the FWI data, estimations of Poisson's ratios are computed for indication of soil types. The Florida Department of Transportation tested this method on computer-based and field experiments and attested to its high potential in geotechnical surface investigation (Tran, et al. 2013).

Microgravity is a relatively new method, which relies on small perturbations of the gravity field due to strong density contrast. It has been shown to effectively predict the locations of voids (Gambetta, et al. 2011). Some may go so far as to describe microgravity as "one of the methods best suited to the detection of voids in the uppermost 20 m, even when these voids are relatively small" (Chalikakis, et al. 2011). However, others have contradictorily reported that the gravity method has poor vertical resolving power (Park, et al. 2010) and is insensitive to voids embedded at depth greater than their size (Tran, et al. 2013).

The Self-Potential signals (also known as Spontaneous Potential) are an electric anomaly generated by the percolation of water. SP surveys give valuable information with respect to the groundwater flow into the vadose zone. However, this technique has previously been combined with other tools and is not intended as a standalone method (Jardani, et al. 2007).

The six geophysical methods described above vary in many ways, but all have in common a sizeable cost and a black box nature in the extrapolation of their results. The latter two explain the need for a device made of affordable components, which allows for a deeper understanding of its functioning.

2.3. The benefits of electrical resistivity methods

ER surveys have been used to investigate soils for over a century. They rely on the simple principle that the electrical resistivities of surrounding soils and rocks alter the distribution of electrical potential in the ground. It works best for fairly conductive earth materials that contrast in resistivity values. Therefore, ER is well suited for the analysis of karst terrain made of clayey soils and carbonate rocks as the two allow for ionic transport, and differ greatly in their concentrations of interconnected pore spaces.

Traditional resistivity methods consist of four electrodes linearly placed in the ground (figure 2). A portable battery is used to deliver a direct-current (DC) between the current source *A* and sink *B*. While the intensity of the current is measured using an ammeter, the voltmeter connected to electrodes *M* and *N* senses the potential difference induced in the earth. It is important to use four electrodes so that current sensors and voltage sensors do not overlap. Otherwise, one

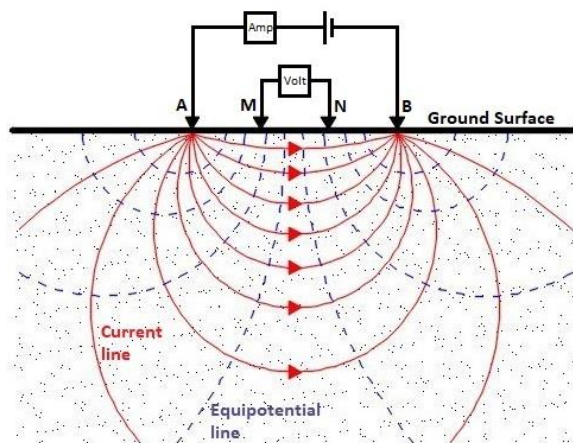


Figure 2. Conventional resistivity analysis of the subsurface using electrodes uniformly spaced in a line according to Wenner array (adapted from Sharma, 1997)

may end up measuring the quality of the electrode contacts instead of measuring the voltage drop across a current flow. Following Ohm's law, the earth's resistance is computed based on the current drawn and the voltage drop between the potential probes. However, the resistance is entirely dependent on the setting of a particular measurement. The intrinsic property of resistivity is found using the resistance and a factor that accounts for the geometry of the electrode array (Zhou, Beck and Stephenson, 2000). Note that the measure found is the apparent resistivity produced by the combination of material(s) over which the voltage drop is measured. As such, it could be only equal to the true resistivity in the investigation of a homogeneous medium. Otherwise, one must keep in mind that it is "definitely not an average value" of the materials with different properties it crosses (Telford, Geldart and Sheriff 1990).

To assess the resistivity at different depths of a particular location and perform a Vertical Electrical Sounding (VES), the electrodes are spread further apart after each reading.

Alternatively, in order to conduct a unidimensional Constant Separation Traversing (CST) at a single depth of interest, the four electrodes are maintained at constant spacing and moved along a horizontal line (Roth and Nyquist 2003).

The development of ER equipment using multiple electrodes and a switching device made it possible to perform large exploration without moving electrodes between measurements (Hiltunen and Roth 2003). In addition to speeding up the process, the use of multi-electrode ER systems and inversion software enabled ER measurements at different depths along a profile and resulted in two-dimensional ER sections (Nyquist, Peake and Roth 2007).

Furthermore, parallel sections are sometimes combined together to produce pseudo three-dimensional datasets. But, when dealing with heterogeneous media, it is recommended to use intersecting sections to ensure coherent results from different directions (Carriere, et al. 2013). Ideally, a true 3D survey is conducted over a grid made of numerous cross-lines so as to minimize any discrepancy (Yang and Lagmanson 2006).

In the literature, the applications of ER methods to karst terrain proved to be very successful in detecting subsurface cavities (Farooq, et al. 2012), locating flooded and air-filled conduits (Zhu, Currens and Dinger 2011; Land 2012), as well as delineating weathered zones and concealed flow paths (Mitrofan, Povara and Maftciu 2008; Kaufmann, Deceuster and Quinif 2012).

The improvements brought to ER methods in the last two decades have called for more complex devices and greater computational efforts. To conduct an ER survey, one has no choice, but to engage expensive professional services. The equipment alone costs around \$1000 per week (Chalikakis, et al. 2011). Therefore, researchers have been working on the implementation of more affordable and intuitive ER devices capable of obtaining the reasonable level of accuracy sought by professionals conducting independent field investigations.

2.4. The fabrication of low-cost ER meter

John Stanley was among the first ones to construct a simple ER meter for “a mere fraction of the price of commercial units” (1981). A voltmeter, an ammeter and four electrodes were the bulk of his design. His device was capable of performing VES to an effective depth of around 15 meter. However, his field data had to be reported by hand on log/log graph paper and interpreted thanks to, now disused, standard resistivity curves. Twenty years later, a very similar device was reproduced with a cost under \$350. This time, a DC to AC power converter was implemented to avoid the polarization of the subsurface material. Through a series of tabletop and field experiments, this inexpensive ER apparatus proved to be capable of “performing resistivity surveys [...] over a wide range of depths” (Herman 2001). When compared to commercial instruments, the same apparatus showed a fairly good degree of correlation (Badmus and Kilasho 2013).

Rather than purchasing commercially available multimeters, Robert Beck (1997) and John Becker (2003) were the first two to opt for microcontrollers wired to different programmable Integrated Circuits (IC). Becker managed to reduce by half the list of components previously required by Beck, but the fabrication of his device was still out of reach of those with little background in electronics. Note that both of their designs primarily served the purpose of archaeological explorations and used a different ER approach with only 2 probes.

Later developments in the field of low-cost ER meters saw the implementation of state-of-the-art ICs in their designs. Two recent papers described the design, construction and test run of user-friendly ER meters. The device designed by Mikailu et al. (2015) generated an Alternative Current (AC) for injection into the soil, which required numerous ICs to sense, oscillate, rectify and amplify the current. The device’s accuracy was then only assessed on simple test circuits. The most recent work by Juhari et al. (2017) proposed a small-scale prototype that focused on DC resistivity surveys. Similarly, its workability was only demonstrated against homogeneous soil samples, and its accuracy in practical settings remains to be determined. Therefore, the fabrication of low-cost ER has to be continued, further tested, and applied to karstic environments.

3. DEVELOPING A LOW COST ER METER

The current work builds upon some of the last designs of ER meters (Becker, 2003; Mikailu et al. 2015; Juhari et al., 2017). Similarly, the proposed prototype implements state of the art technology by integrating a microcontroller and programmable modules. However, this study simplifies some of the previous designs so as to become easier to assemble and intuitive to operate, while maintaining the same level of accuracy. The functioning of the developed device is described part by part hereunder. The reader may refer to figure 5 to see how each individual component fits into the whole.

3.1. Development boards

With a unit cost barely exceeding \$10, development boards such as the Arduino Uno have become widely available (figure 3). They consist of a microcontroller (1) preassembled on a board that is connected to multiple Input and Output (I/O) pins. By connecting the board to a computer through the USB port (2) and using the open-source Integrated Development Environment (IDE), the user can write a program, often referred to as a sketch, which continually loops to repeat a series of commands. The IDE only requires the user to define the “setup” and “loop” functions. With a sketch composed of

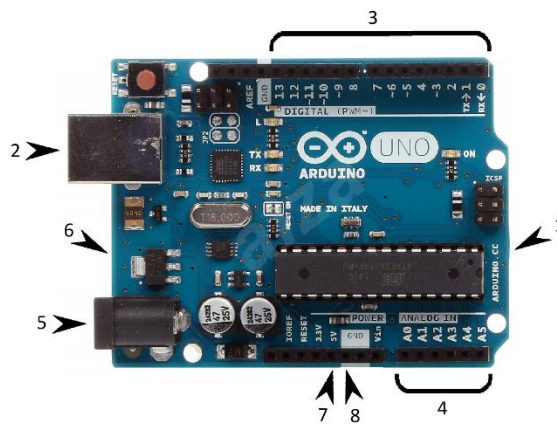


Figure 3. Arduino Uno development board consisting of (1) microcontroller, (2) USB port, (3) digital pins, (4) analog pins, (5) barrel jack, (6) voltage regulator, (7) power supply, and (8) ground

a few lines of code written in the C or C++ language, a non-programmer can access the numerous functions of the microcontroller. In addition to its flexible software and supportive online community, the main advantage of the Arduino board while creating a prototype is its intuitive hardware. Depending on the task, one chooses different types of I/O pins. For example, the 14 digital I/O pins (3) have the capabilities of reading and writing binary signals. They understand 0V as a binary 0, and 5V as binary 1. Therefore, they are able to do things such as powering an LED or sense if a button is pressed. Contrarily, the 6 analog inputs (4) are mostly used to read analog sensors with varying signals anywhere between 0 and 5V. The board itself is typically powered with batteries via the barrel jack

(5) and uses a voltage regulator (6) to provide the different modules with a constant power supply (7) and sink (8). Note that exposing the input pins to any voltage greater than 5 volts or any currents greater than 40 mA may cause damage to the board.

3.2. Analog inputs

3.2.1. Ammeter

The initial step in the fabrication of an ER meter was the implementation of an accurate current sensor. Current sensors that rely on Ohm's law were found to be the most suitable for this project. They typically consist of a resistor of known resistance. When the sensor is connected in series with the load of interest, it measures the voltage drop across the known resistor. From there, it is simple to calculate the current drawn by the load. However, a resistor placed in series with a load has the undesirable effect of dropping the voltage that is applied to that load. Consequently, only a resistor of very low resistance, also known as a shunt resistor, must be placed in the current path not to disturb the circuit. But the marginal drops in voltage caused by shunt resistors are hardly noticeable. To increase the magnitude of the signal by a set gain, a precision amplifier is typically used to measure the voltage drop across the shunt resistor. Integrating both a 0.1 ohm resistor and a precision amplifier, the Adafruit INA219 bi-directional DC current monitor was chosen for this design. Its resolution of 0.1 mA and its range of ± 400 mA (at 16V) met the level of accuracy sought for a current meter (Telford, Geldart and Sheriff 1990). However, note that the maximum gain error for INA219 IC is 0.5% in addition to a maximum current measurement error of 0.5% at 25 degrees Celsius.

3.2.2. Voltmeter

The second step in the fabrication of an ER meter was the creation of a voltmeter that could accurately measure voltage drops between two electrodes. Because the voltages of interest would likely exceed 5V, the input voltage had to be scaled down. To this end, a two-resistor voltage divider was implemented. Every time the two leads (+, -) are in contact with a circuit, the voltage divider is placed in parallel across the current path (figure 4). The voltage

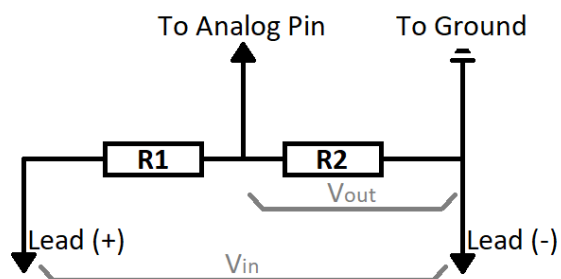


Figure 4. Inner workings of an analog voltmeter made up of a two-resistor voltage divider

drop across the two resistors R_1 and R_2 is then equal to V_{in} while the sought voltage drop across R_2 is V_{out} .

Connected to the middle of this voltage divider, the analog pin reads a value that is only a fraction of the input voltage. The latter can be demonstrated based on the common current found in a series of resistors.

$$I_{1,2} = I_2$$

Based on Ohm's law, the current across the meter is equal to the ratio of the input voltage to the sum of the resistance.

$$\frac{V_{in}}{R_1 + R_2} = \frac{V_{out}}{R_2}$$

By solving for the output voltage, the following is obtained:

$$V_{out} = V_{in} \times \frac{R_2}{R_1 + R_2}$$

To a certain extent, most gauges disturb the system they measure. This holds true for a voltmeter. Because the latter is always connected in parallel with the load it measures, it draws current from the load and lowers the equivalent resistance of the circuit as follows:

$$\frac{1}{R_{equivalent}} = \frac{1}{R_{load}} + \frac{1}{R_{voltmeter}}$$

An important consideration when choosing a pair of resistors for the fabrication of the voltmeter was to minimize the disturbance caused to the system. To reduce this loading effect, Telford, Geldart and Sheriff (1990) recommended using a voltmeter of impedance greater than 1M ohms. Therefore, a combination of 1M- and 100k-ohm resistors were used for R_1 and R_2 , respectively. In spite of these efforts, it is important to realize that a minor loading effect persisted. The latter cannot be accounted for, nor rectified in a systematic fashion as the ratio to other loads in the system typically remains undetermined. Overall, the loading effect generated by the voltmeter (of great internal resistance) would remain marginal for the range of interest of relatively much lower resistances (table 1). Therefore, the voltmeter showed the ability to properly perform on the range of resistances typically encountered in the field.

Table 1. Theoretical resistance across standard loads placed in parallel with a high-impedance voltmeter

True Resistance (ohm)	Equivalent Resistance (ohm)	Percent Change due to Loading Effect
10 ¹	9.9999	0.0009
10 ²	99.991	0.0091
10 ³	999.09	0.0908
10 ⁴	9909.9	0.9009
10 ⁵	91666.7	8.3333

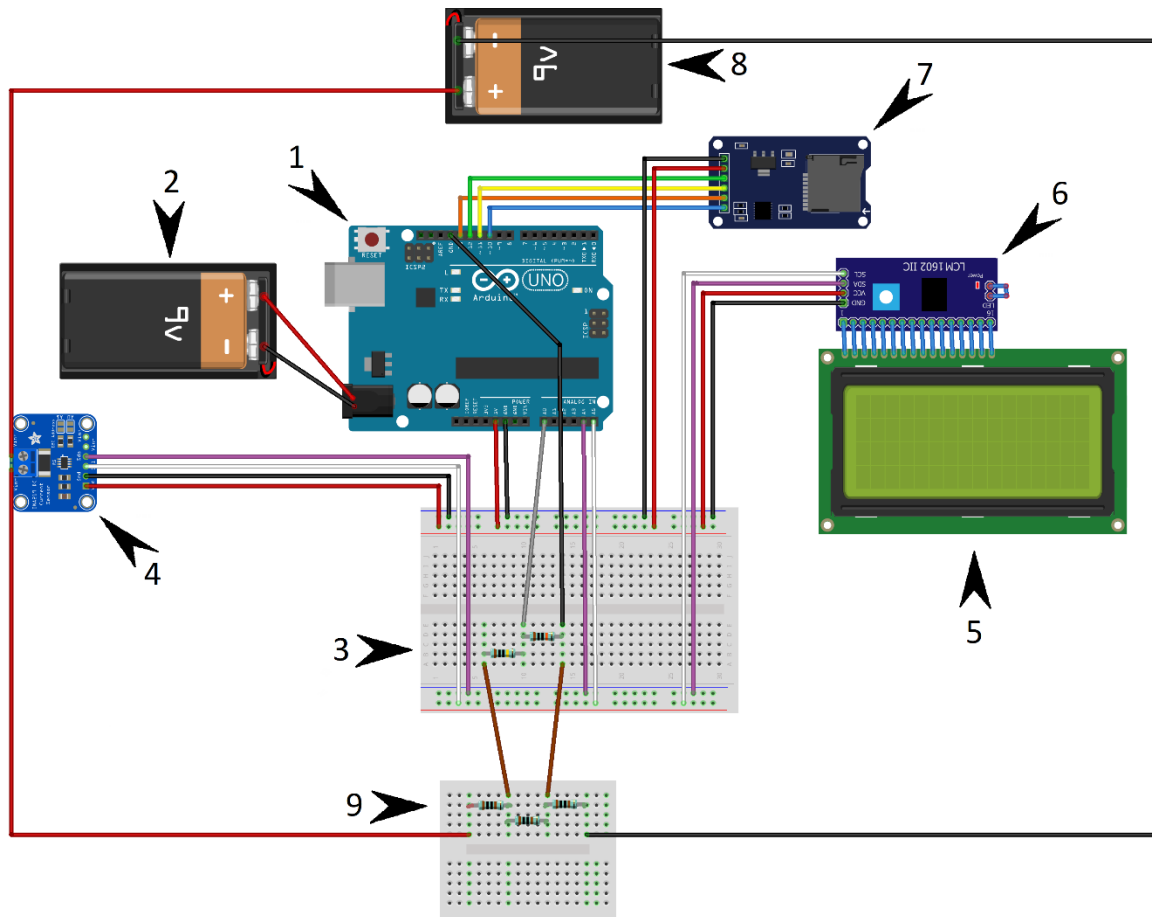
The voltage divider with the characteristics above is capable of scaling down the input voltage by a ratio of 11:1, making the voltmeter suitable for values of up to 55 volts. Formatted to a value between 0 and 5 volts, the analog input voltage is not read by the microcontroller as such. In fact, the signal gets processed by an onboard Analog to Digital Converter (ADC) that returns a 10 bit integer on the range between 0 and 1024. Consequently, one must keep in mind that the resolution of any analog pin on the Arduino Uno is 4.88 mv/count (i.e. $5v \div 1024$ counts).

3.3. Digital outputs

In addition to sensing current and voltage, an ER meter has to display and compile data. To show the readings in real time, a Liquid Crystal Display (LCD) was implemented in this design. An SD card module was added to allow for data compilation and transfer. The device was programmed to record the current, voltage, and resistance measurements in a .csv file. In this file, the top of each column is labeled with the appropriate header for convenience, and a blank space is left every time the device is initiated (see Appendix).

3.4. Interfacing with modules

The Arduino Uno controls the several surrounding ICs, whether they serve as analog inputs or digital outputs. Figure 5 shows the different components mentioned above as well as the ways by which they interact. While the Arduino board (1) is typically powered by an independent 9V DC supply (2), modules are, by contrast, typically connected to both 5V and ground wires (respectively, in red and black) and powered by the board.



fritzing

Figure 5. Wiring of the proposed low-cost ER meter consisting of (1) microcontroller, (2) 9V battery, (3) voltage divider, (4) DC current sensor, (5) LCD screen, (6) I2C module, (7) SD card module, (8) DC power supply, and (9) series of resistors under test.

There exist different ways for the modules to report information to the microcontroller. The simpler one is to communicate a signal directly to an I/O pin. The voltage divider (3) consisting of the 1M- and 100k- resistors (respectively, to the left and right) is wired (in grey) to the analog pin A0.

The INA219 current sensor (4) has a greater amount of information to report. So, it uses a different approach. The Inter-Integrated Circuit (I2C) protocol enables one “master” device to communicate with multiple “slave” ICs over only two signal wires. The master generates the serial clock signals over the SCL wire (in white) while each slave reports back data using a unique address over the SDA wire (in pink). Initially, the LCD (5) required 16 different wires, but an I2C module (6) was added to enable a simpler wiring.

The SD card module (7) interacts in a different fashion by using the Serial Peripheral Interface (SPI) bus. The SPI is a four-wire serial bus that also uses a master-slave architecture. The microprocessor generates a Serial Clock (SLK) signal and identifies the output Chip Selected (CS) using two wires (respectively, in orange and blue). The information from the “master” to the “slave” (MOSI) and vice-versa (MISO) is transferred via two other wires (respectively, in yellow and green). Note that Figure 5 shows an additional 9-V DC supply (8) put in place to create a voltage drop across three 1k-ohm resistors (9) placed in series in accordance with the test setup described in Section 3.6.

Overall, the ICs that make up this prototype measure and process data in ways that are easily explained and understood. Roughly 20 wires and less than eighty lines of uploaded commands are all it takes to assemble this ER meter (see Appendix). Consequently, this straightforward design tackles the issue of the possible black box nature of laboratory equipment described in Section 2.2.

3.5. The inexpensive cost of the design

To emphasize the affordability of the current prototype, an overview of the cost of each component at the time of purchase (i.e. between Nov. 1 2017 and Jan. 16 2018) is shown in Table 2. Note that the unit price of wires, connectors, and resistors is negligible.

Table 2. Cost breakdown of the proposed low-cost ER meter

Component	Unit Price in USD (excl. Sales Tax)
Elegoo Uno R3 board	10.90
LCD 4x20 + I2C module	12.99
SD card module	2.95
INA219 current sensor	11.80
Total =	38.64

3.6. The reliability of the proposed device

In order to prove the concept of the device proposed in Sections 3.1-4, its accuracy was tested on a set of resistors of ohmic values ranging widely, from 30 to 22,000 ohms. Three identical resistors with a 1% tolerance were connected in series to reproduce a medium of uniform resistance. A 9 volt battery was connected at each end to provide an unregulated power supply. The voltage drop was measured over the middle resistor. To capture the potential variations in noise and produce a reliable dataset, 5000 readings of the resistance were collected for each set of resistors and summarized in table 3.

Table 3. Results from confirmatory testing of the proposed ER meter against sets of known resistors

True (+/-1%)	Min measured	Max measured	Median	Mean	SD
30	28.98	29.90	29.46	29.43	0.18
47	45.58	47.39	45.92	46.04	0.34
67	65.91	68.02	66.43	66.35	0.14
100	96.68	99.60	98.14	98.14	0.53
147	142.2	147.0	144.3	144.6	0.8
220	201.9	222.1	214.8	214.4	1.8
320	286.1	318.7	309.4	310.3	1.6
470	451.9	467.8	459.1	458.2	2.8
690	653.9	695.8	680.3	680.7	4.8
1000	948.9	1035.9	981.6	983.1	17.8
1470	1316	1527	1450	1447	20
2200	1983	2768	2190	2150	71
3200	2793	5550	3163	3117	136
4700	3990	5801	4744	4624	247
6900	5479	9668	7117	7010	557
10000	6445	13159	8594	10062	2038
14700	8594	25781	12891	15165	4936
22000	12891	26318	25781	23850	4604

Overall, the mean and median attributes did not depart from one another and were interpreted as evidence of the repeatability of the setup. The mean absolute percent error of the readings was plotted against the true resistance in orders of magnitude (figure 6).

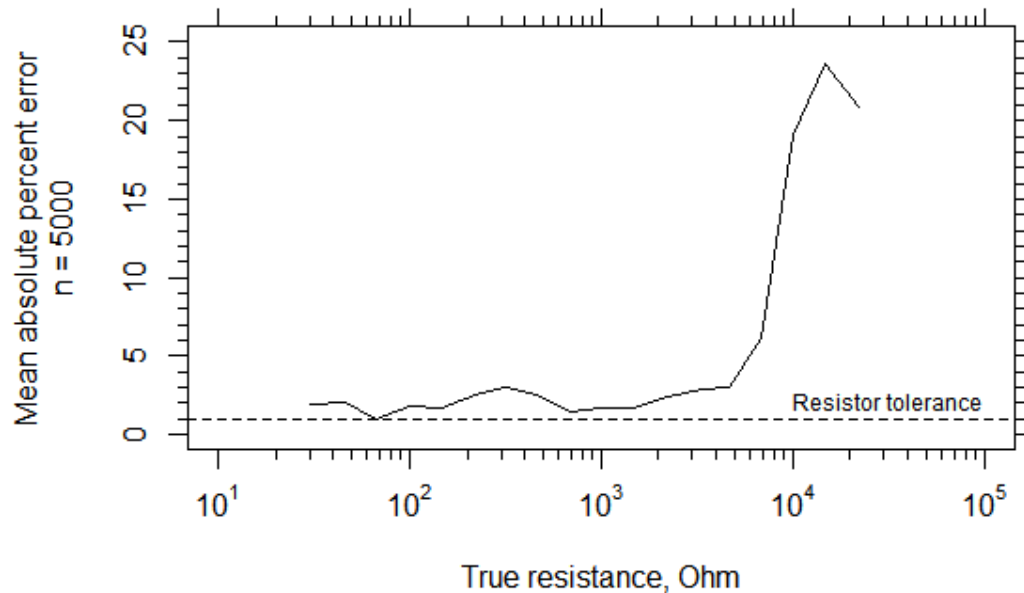


Figure 6. Level of accuracy of the proposed device during confirmatory testing

Between 30 and 4700 ohms, the Mean Absolute Percent Error (MAPE) was stable, with values ranging between 1 and 3%. These numbers agreed with the resistor tolerance and the specifications of the current sensor. They also implied that the noise in these 5000 readings was not significant and did not affect the MAPE.

However, when performing in circuits with a total resistance equal to or greater than 20700 ohms, the device returned higher MAPE values. According to Ohm's law, when a circuit is exposed to greater resistances, the current drawn from a constant power supply decreases. With values of current approaching the sensitivity of the sensor (i.e. 0.1 mAmps), more readings became less accurate and the MAPE increased sharply.

The relationship between the variations in the dataset and the levels of current was further studied. An indicator of the dispersion in a distribution is the Relative Standard Deviation (RSD). The RSD is defined as the ratio of the standard deviation to the mean. The levels of current were calculated as the ratio of the theoretical amplitude of the current in the circuit to the manufacturer reported sensitivity of the sensor. A plot of the logarithm of the resistance relative standard deviation as a function of the logarithm of current amplitude to sensitivity ratio yielded a robust linear fit of negative slope 0.70 (figure 7).

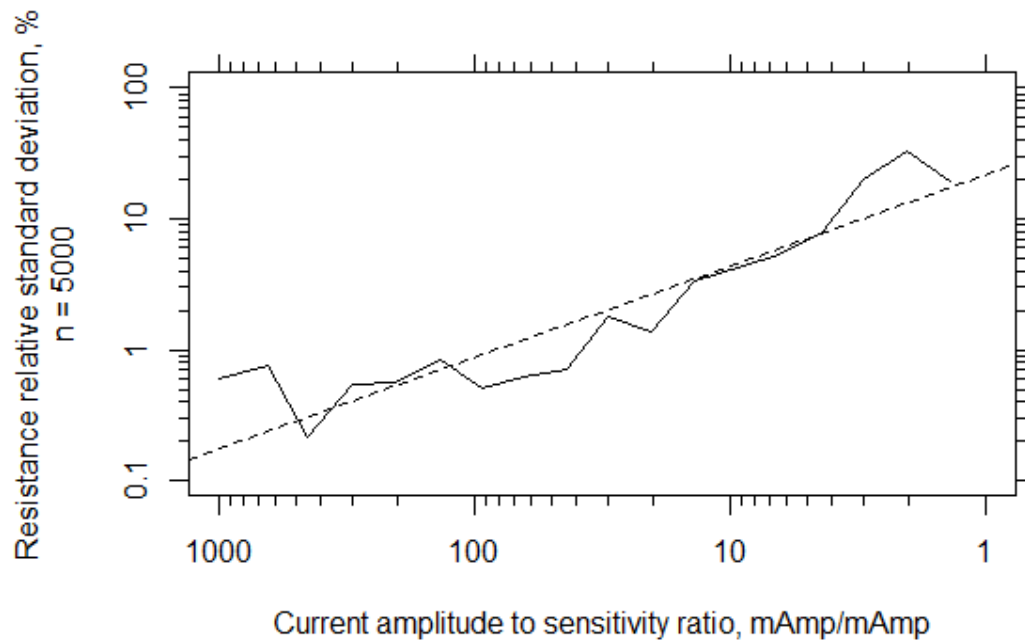


Figure 7. Exponential relationship between variations in resistance readings and current levels as shown by the dashed line of robust linear fit $a=1.34$ and $b=-0.70$

In order to study the strength of the supposed linear association, the normality between the two datasets was first considered. Shapiro-Wilk normality tests were performed on both of them. With p-values of 0.648 and 0.076 that exceeded the alpha level of 0.05, the null hypothesis that the samples came from normally distributed populations could not be rejected. This result was corroborated by the visual inspection of Q-Q plots. Assuming normal sample distributions, the association between the two variables was characterized using Pearson's method. The correlation coefficient and p-value of -0.916 and $9.94e-08$, respectively, showed the strong association as well as the high statistical significance of the relationship between the variations in the resistance readings and the levels of current (figure 8).

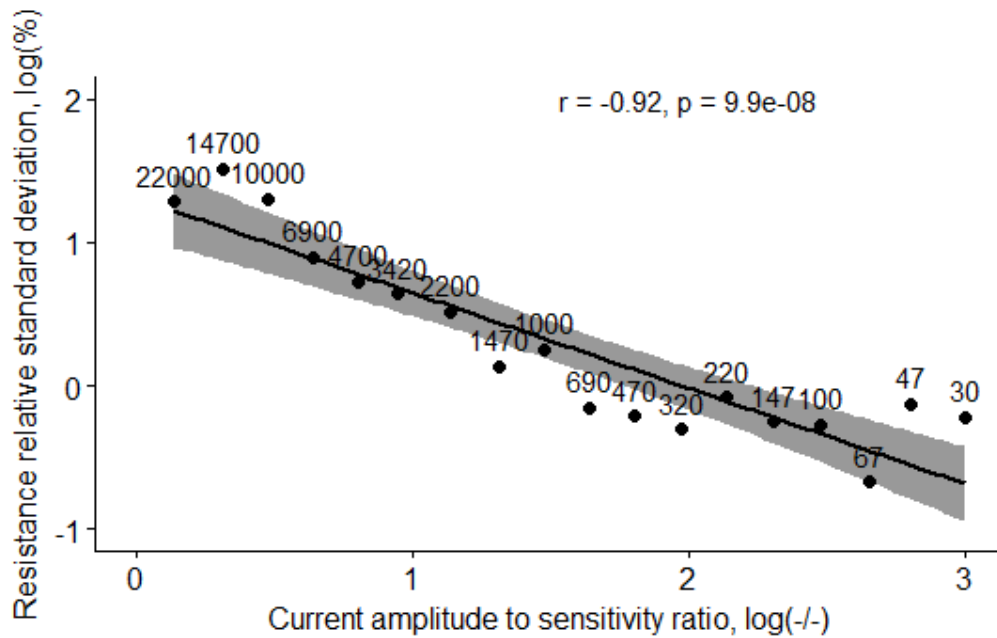


Figure 8. Strong negative correlation between the variations in the resistance readings and the levels of current for the different values of resistance (Ohm). The shaded region represents the confidence interval of the correlation coefficient at 95%

Consequently, it is reasonable to link the greater levels of noise and the peak in the MAPE to relatively low values of current in the circuit, rather than to the overall accuracy of the device. This also highlights the importance of the voltage delivered by the power supply to the system. The greater the voltage in play, the greater the current measurement, and the more confident the observer can be in the precision of the device.

Considering that the resistivity values of different materials vary by orders of magnitude, the MAPE was negligible for as long as appropriate power was supplied, and the device showed a satisfactory level of accuracy and precision.

4. Methodology

During the confirmatory testing described in Section 3.6, the device measured wide-ranging values of current and potential with a great level of accuracy. The device should next be applied to soil test beds to study its reliability in the context of soil surveys.

4.1. ER theory

In an effort to remain affordable and intuitive to use, this study implemented a conventional four-electrode resistivity meter. The first dipole served to inject a current into the ground, and the second one, to measure the equipotential values induced along hemispherical surfaces (figure 2). Different electrode sequences were developed as much for field efficiency as for their accurate results (Nyquist, Peake and Roth 2007). In karst

surveys, three arrays are commonly used to investigate the underground: Wenner, Schlumberger, and dipole-dipole. The symmetry of Wenner array made it the

Table 4. Electrode array configuration (adapted from Samouëlian et al., 2005)

Wenner	A \xleftrightarrow{a} M \xleftrightarrow{a} N \xleftrightarrow{a} B
Schlumberger	A $\xleftarrow{\dots b}$ M \xleftrightarrow{a} N $\xleftarrow{\dots b}$ B
Dipole-dipole	A \xleftrightarrow{a} B \xleftarrow{na} M \xleftrightarrow{a} N

most straightforward to compute and therefore, relevant to this work (table 4). In addition, a part of this study considered the use of the dipole-dipole array, recognized by many to provide the greatest sensitivity to karst features (Zhou, Beck and Adams, 2002; Hiltunen and Roth, 2003; Land, 2012; Farooq et al., 2012).

The literature contains numerous (more and less) complex demonstrations of earth resistivity calculation. The following explanations are adapted from the work by Telford, Geldart and Sheriff 1990) as well as Samouelian, et al. (2004). Electrodes A and B are the power supply and sink, respectively. Electrodes M and N are the potential dipole. Essentially, a potential $V_{M,A}$ is induced at point M that is at a given distance r_1 from the power supply A of current (I) at the surface of a medium of apparent resistivity (ρ) as given by:

$$V_{M,A} = \frac{I\rho}{2\pi r_1}$$

In addition, the potential ($V_{M,B}$) induced at point M by the power sink B (of equal intensity but opposite direction) that is at a distance r_2 away is:

$$V_{M,B} = \frac{-I\rho}{2\pi r_2}$$

The net potential measured by electrode M is the sum of the previous two:

$$V_{M,A} + V_{M,B} = \frac{I\rho}{2\pi} \left(\frac{1}{r_1} - \frac{1}{r_2} \right)$$

The net potential at a point N that is a distance r_3 and r_4 away from current supply and sink, respectively, is evaluated similarly. For the conventional arrays of interest, the difference in potential across two electrodes is considered. The lengthy terms depending upon the electrode arrangement can be replaced by a geometric factor K .

$$\Delta V = \frac{I\rho}{2\pi} \left[\left(\frac{1}{r_1} - \frac{1}{r_2} \right) - \left(\frac{1}{r_3} - \frac{1}{r_4} \right) \right] = \frac{I\rho}{K}$$

By solving for apparent resistivity, the following is obtained:

$$\rho = \frac{K\Delta V}{I}$$

The geometric factor for the uniformly spaced Wenner array can be easily evaluated by replacing the distances r_1 and r_4 by a term a and the separations r_2 and r_3 by twice as much (table 4).

$$K_{Wenner} = \frac{2\pi}{\left(\frac{1}{a} - \frac{1}{2a} \right) - \left(\frac{1}{2a} - \frac{1}{a} \right)} = 2\pi a$$

For the dipole-dipole array, both the current dipole spacing and the potential dipole spacing are held at a constant length a , and the separation between the dipoles is a multiple n of length a (table 4). Its geometric factor is expressed as follows:

$$K_{dipole-dipole} = \frac{2\pi}{\left(\frac{1}{na} - \frac{1}{a(n+1)} \right) - \left(\frac{1}{a(n+1)} - \frac{1}{a(n+2)} \right)} = \pi n(n+1)(n+2)a$$

The conventional unit of apparent resistivity is Ohm-m. The resistivity reading associated with a certain electrode sequence and spacing yields a specific depth of investigation. For the dipole-dipole array (frequently used to perform combined sounding-profiling survey), each apparent resistivity reading is plotted "at the intersection of 45-degree lines from the

sender and receiver along the line” (Hallov 1957). In the case of Wenner array, Herman (2001) demonstrated that the effective depth of a measurement takes a simple mathematical form equal to half the spacing between the current dipole (i.e. $\frac{3a}{2}$).

A straightforward method to interpret measurements obtained from a one-dimensional VES is to plot the apparent resistivity with respect to the depth of investigation to the center of the survey line. A logarithmic scale is often used to accommodate the large range in resistivity values. A change in the trend of the plotted results generally indicates the presence of a medium with different electrical properties. The quick analysis of such a plot enables the observer to identify the number of soil layers as well as evaluate their respective resistivity and thickness. The data resulting from the survey of a floodplain was plotted to serve as an example (figure 9). Within the first meter of soil surveyed, the resistivity values appeared to fall to about 100 Ohm-m, where it remained constant for the next 3m. It then hit another large medium of higher resistivity. These different observations were consistent with the knowledge of the site: a dry topsoil, a layer with potential groundwater occurrence; and a bedrock at an expected depth of 4m.

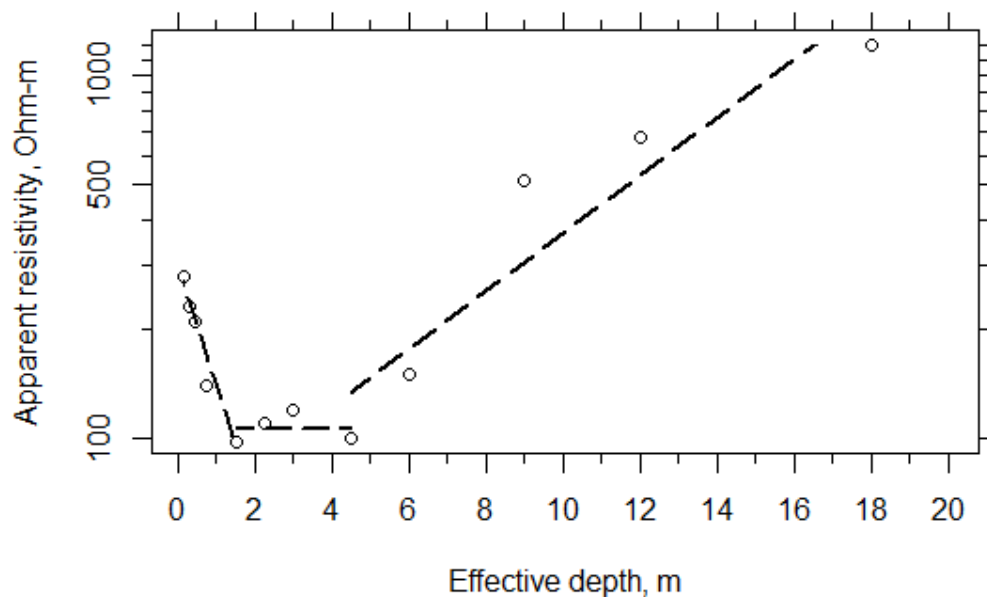


Figure 9. Floodplain resistivity survey (values obtained from Herman, 2001)

Multiple functions exist to analyze curves, perform linear segmentation, and recognize the breakpoints of interest. The weakness of these diagnostic tests lies in their need for a cutoff value, such as an angle tolerance or a certain standard deviation from a given observation. The implementation of such functions proved to be inefficient as it required adjustments to be made when dealing with surveys of varying extents as well as underlying systems with different properties. After making arbitrary assumptions, it appeared that the diagnostic did not add information other than what was already obvious and, at times, tended to be sensitive to the noise present in earth surveys. Even more advanced analysis of one-dimensional VES data, such as the IP2Win inversion software, require to input the numbers of layers and to approximate resistivity values in order to produce the depth sounding model associated with the least error. Consequently, plotting the apparent resistivity against the effective depth was the most effective approach to interpret VES measurements, and was applied throughout this study.

In the scope of this study, two experiments were conducted in a tabletop laboratory setting to ensure the proper functioning of the proposed device and its overall potential to assess karst-prone sites. The first one served to evaluate the accuracy of the information provided by the depth sounding of soil layers characteristic of karst terrains. The second one studied the ability of the device to detect the presence of a void along a profile.

The soil used in both setups was borrowed from a local construction site along Maury Ave. in Charlottesville, VA. The red fine-grained soil was dug in January 2018 in the process of foundation excavation work. Geotechnical testing (in accordance with ASTM D2487) found 74 percent by weight of fines, a liquid limit of 58, and a plastic index of 18. Based on the Unified Soil Classification System (USCS), these properties revealed the presence of an elastic silt with sand (MH).

4.2. Experiment One

The first setup was intended to reproduce a karst environment composed of a layer of soil underlain by a weathered bedrock. A roughly equal mix of marble stones and elastic silt was placed at the bottom of a 12-gallon plastic storage container (54cm L x 37cm W x 28cm H) and compacted to height of 9 cm. It was then covered with 12 cm of compacted elastic silt (figure 10). The temperature of the mix was uniformly 20 degrees Celsius and the moisture content of the soil was similar to its field condition (22 percent by weight).

A first survey line was placed along the length of the box. A current was delivered to one dipole, and the potential was measured using another. The VES of the depth to the center of the survey line was performed with Wenner array initially, and later using the dipole-dipole configuration. In 10 seconds, 50 readings of current and potential relative to a specific setup were collected and averaged. The probes were incrementally spread in order to sound greater depth (figure 11). To ensure the reproducibility of the results, a second VES was conducted along a survey line parallel to the first one and offset by 6cm.



Figure 10. Karst terrain underlain by weathered limestone bedrock reproduced in a tabletop laboratory setting

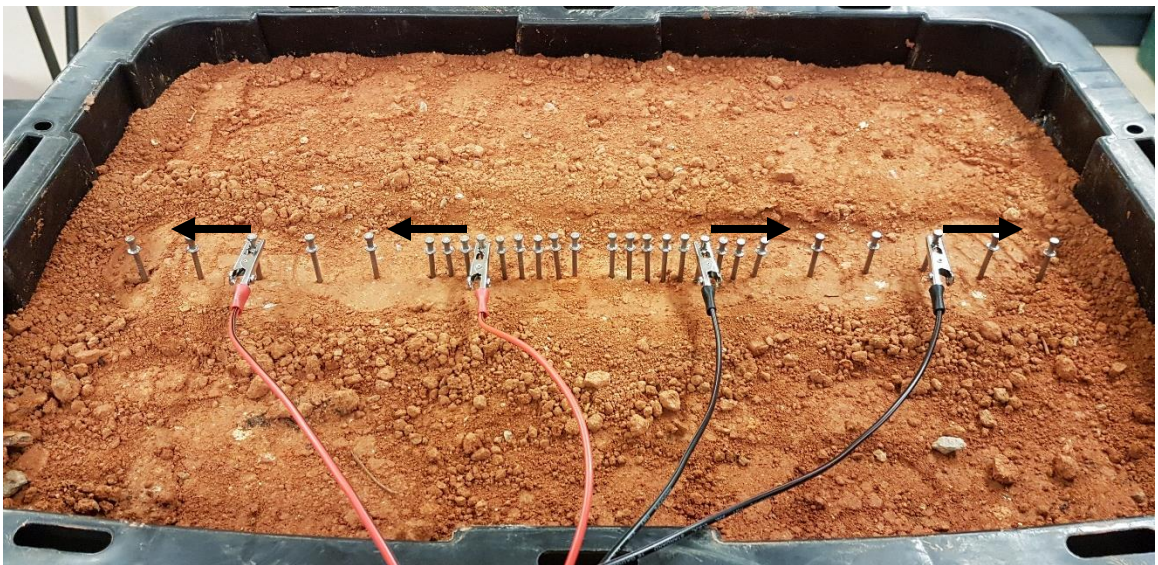


Figure 11. VES performed by progressively spreading the electrodes of a Wenner array in a tabletop setting

4.3. Experiment Two

The second setup was intended to study the ability of the device to detect the presence of a vertical feature prone to cause disruptions along a horizontal profile. To simulate an air-filled void of high resistivity, a piece of foam board (10cm L x 10cm W x 10cm H) was taped to the bottom of a plastic container (60cm L x 43cm W x 45cm H). The container was filled with elastic silt to a compacted height of 15cm. The temperature of soil was uniformly 20 degrees Celsius and the moisture content of the soil was similar to its field condition (22 percent by weight). Horizontal profiles were generated by CST using Wenner array. The four electrodes were maintained at a 5cm-spacing and shifted along a traverse line, resulting in a resistivity profile 7.5 cm beneath the surface. Two 7-Ah rechargeable batteries were connected in series to supply a 24V direct current to the outer current dipole. Previous to the recording of any measurement, several drops of water were poured around each probe to alleviate contact resistance. Measurements of current and potential were taken at 6 stations, at increments of 5 cm along the profile. These measurements served to calculate the apparent resistivity relative to the center of the CST. The void was located on center, at the extremity of the first profile, and extended 5 cm in x-y directions (figure 12a). Four additional profiles at similar depths of investigation were traced by incrementally shifting the whole array 5 cm to the right (figure 12b), resulting in a matrix of results. In the first two profiles, the results at the last station were expected to reveal the void buried under 5 cm of soil. The longitudinal effect of the void on other data points was undetermined. The implementation of 5 profiles served to determine the background resistivity in places unaffected by the presence of the void.

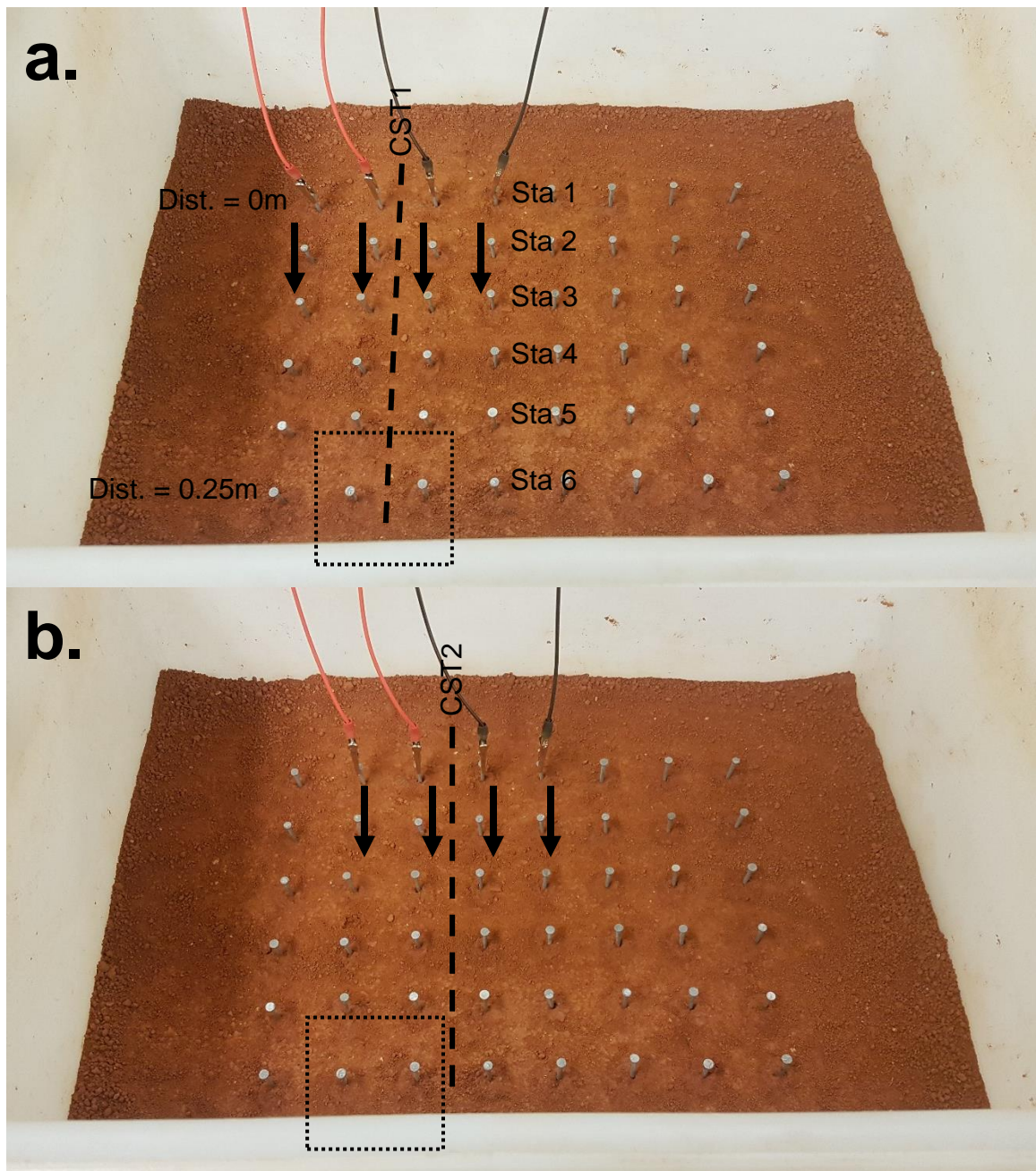


Figure 12. CST along a profile (dashed line) intercepting a void buried under 5 cm of soil

5. Results and discussion

5.1. Experiment One

The initial use of a single 12v power supply proved to be unsuccessful because it produced high levels of noise that led to unusable readings. Thereafter, two 7-Ah rechargeable batteries were connected in series to supply a 24V direct current to the current dipole and enable the measurement of valid answers. After careful analysis of the distribution in the readings, it was found that there was no skewness resulting from this relatively higher direct current, and that the effects of a potential ground polarization were negligible.

Using the Wenner configuration, the VES of two close points were performed along parallel survey lines. Both surveys sounded a similar underground consisting of a 12-cm-thick silt layer underlain by an artificial horizon of fissured limestone. In each survey, 50 readings of the current and potential were taken and averaged with respect to the effective depth (table 4).

Table 5. Tabletop resistivity measurements of VES1-2

a (cm)	z (cm)	VES 1			VES 2		
		I (mA)	V (V)	ρ (Ohm m)	I (mA)	V (V)	ρ (Ohm m)
2	3	1.88	2.80	187	2.01	4.33	271
3	4.5	1.68	2.24	250	1.88	3.82	384
4	6	1.60	1.87	293	1.79	3.18	446
5	7.5	1.59	1.80	354	1.69	2.64	492
6	9	1.36	1.16	321	1.70	2.17	481
7	10.5	1.58	1.48	412	1.80	2.14	525
8	12	1.56	1.13	366	1.58	1.56	495
9	13.5	1.52	1.13	421	1.48	1.19	454
10	15	1.40	0.78	347	1.52	1.25	518
11	16.5	1.39	0.76	378	1.53	1.13	511
12	18	1.40	0.80	431	1.51	1.08	539
13	19.5	1.41	0.81	467	1.35	0.97	591
14	21	1.33	0.67	441	1.21	0.71	513
15	22.5	1.20	0.51	400	1.21	0.76	590
16	24	1.24	0.76	619	1.19	0.81	682
17	25.5	1.21	0.81	715	1.10	0.66	647

The values of apparent resistivities for both surveys were plotted on a logarithmic scale against the effective depth (figure 13). Overall, both surveys followed the same pattern and the changes in trends somewhat aligned with the expected layer depths. Resistivity values increased until reaching the mix of marble stone and silt. As soundings penetrated the second layer, the values were fairly constant. Once the depth of investigation reached the bottom of the test bed, the resistivity values peaked in reaction to the low conductivity of the plastic box.

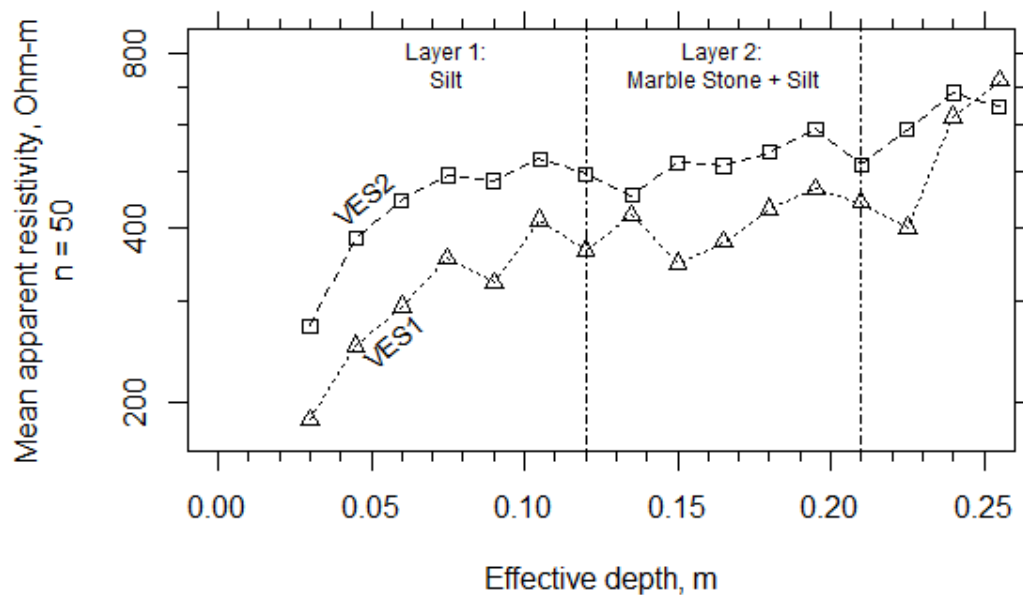


Figure 13. VESs of a test bed containing an artificial layer of fissured limestone between the depths of 12 and 21 cm

A closer look at the first survey highlighted the obvious changes in patterns along the first VES curve (figure 14). The latter coincides with the depths to the top and bottom of the soil layers in the test bed under study. Moreover, when sounding the mix of marble stone and silt, the device found a constant mean value of around 407 Ohm-m, which fits in the range of resistivity values expected for fissured limestone (Telford, Geldart and Sheriff, 1990; Reynolds, 1997; Nordiana, et al., 2013).

As for the second survey (figure 15), the general trend remained similar, with two exceptions. First, the assessment of the first layer's thickness did not yield as accurate of a result (0.07m instead of 0.12m). Secondly, the resistivity found while probing the artificial horizon of fissured limestone was somewhat greater with an averaged value of 512 Ohm-m, but still in agreement with the expected range.

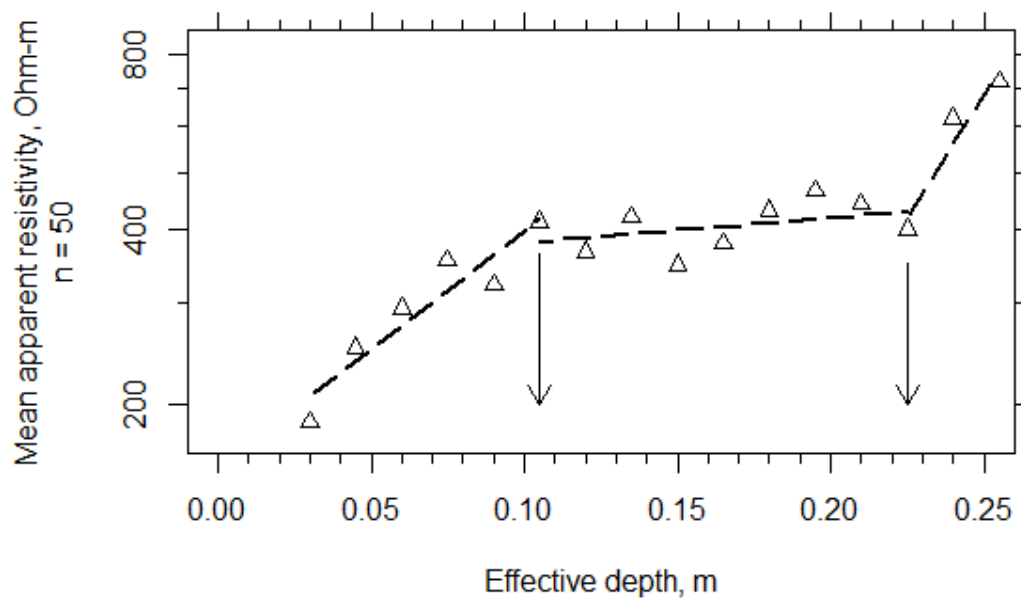


Figure 14. VES 1 indicating a potential limestone layer of apparent resistivity of 407 Ohm-m between 11 and 23 cm

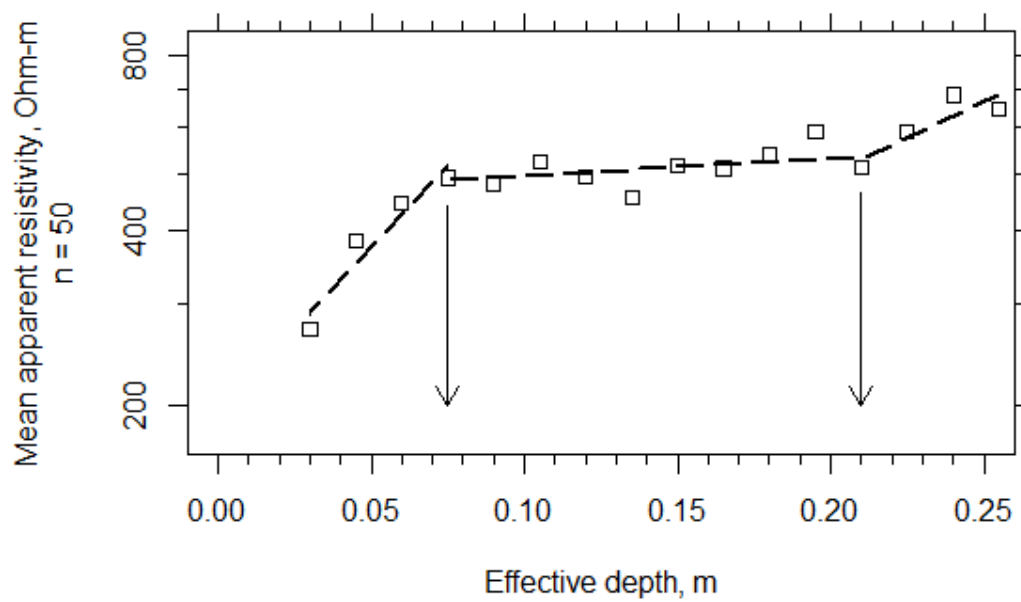


Figure 15. VES 2 indicating a potential limestone layer of apparent resistivity of 512 Ohm-m between 8 and 21 cm.

Finally, the datasets produced by the two consecutive VES surveys were compared in order to assess the extent of their association. Based on the outcome of Shapiro-Wilk normality tests (i.e. p-values of 0.19 and 0.53 for VES 1 and 2, respectively), the null hypothesis could not be rejected. Since both samples somewhat followed a normal distribution, the association between the two datasets was measured using Pearson's method. It was found that the two datasets were significantly correlated by a coefficient of 0.881 and a p-value of 6.50×10^{-6} (figure 16). This showed that the soundings at two locations separated by several centimeters yielded replicable findings.

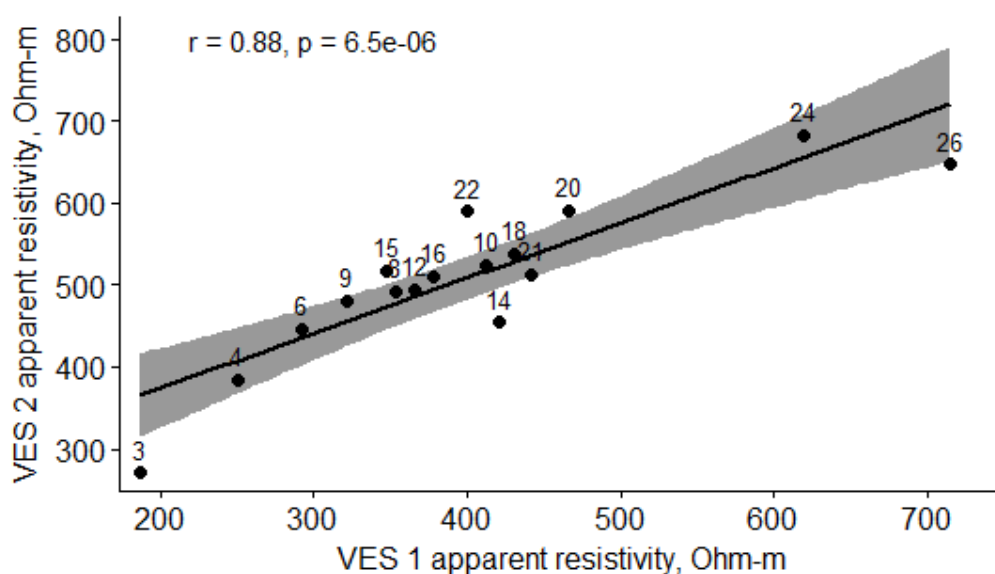


Figure 16. High repeatability based on the strong positive correlation between the two VES datasets at the different effective depths (cm). The shaded region represents the confidence interval of the correlation coefficient at 95%

Note that attempts to repeat these surveys using the dipole-dipole array were made, without success. The device did not measure any values of potential induced by the current dipole. Due to its low signal-to-noise ratio, this array proved to be unusable in this study.

5.2. Experiment Two

CST surveys were performed to determine the lateral variations of resistivity produced by a buried void. The current and potential induced were measured at 6 stations at increments of 5 cm along a profile.

This CST procedure was repeated to produce in total five different profiles. The apparent resistivity values to an effective depth of 7.5cm were calculated based on the Wenner array (table 5).

Overall, most values of apparent resistivity fell within a range of 375 to 500 Ohm-m. Note that this range agreed with the VES measurements made of the same soil to an effective depth of 7.5cm in Section 5.1 (i.e. 354 and 492 Ohm-m). The resistivity values at the tail of the first and second profiles appeared relatively higher. To visualize the lateral variations caused by the void, the apparent resistivity values of all CSTs were plotted on a logarithmic scale against their respective distance along the profile (figure 17). This highlighted the clear disruption caused by the void on the two profiles closer to it (i.e. CST1-2). Apart from that, the rest of the values illustrated the typical noise encountered in ER surveys.

Table 6. Tabletop resistivity measurements of CST1-5

z=7.5cm	Dist. along profile (cm)	I (mA)	V (V)	ρ (Ohm m)
CST 1 (Offset=0cm)	0	1.2	1.696	444
	5	0.9	1.128	394
	10	0.8	1.021	401
	15	1	1.343	422
	20	0.8	1.450	569
	25	0.8	1.880	738
CST 2 (Offset=5cm)	0	1.2	1.752	459
	5	1	1.343	422
	10	0.9	1.235	431
	15	0.9	1.289	450
	20	0.8	1.235	485
	25	0.8	1.772	696
CST 3 (Offset=10cm)	0	1	1.308	411
	5	1	1.396	439
	10	1	1.289	405
	15	1.1	1.611	460
	20	1	1.450	456
	25	1	1.396	439
CST 4 (Offset=15cm)	0	0.9	1.391	486
	5	0.9	1.289	450
	10	1.1	1.504	430
	15	1.2	1.719	450
	20	0.9	1.182	413
	25	1	1.504	472
CST 5 (Offset=20cm)	0	1	1.343	422
	5	1	1.289	405
	10	1.1	1.558	445
	15	1	1.235	388
	20	0.9	1.128	394
	25	1	1.396	439

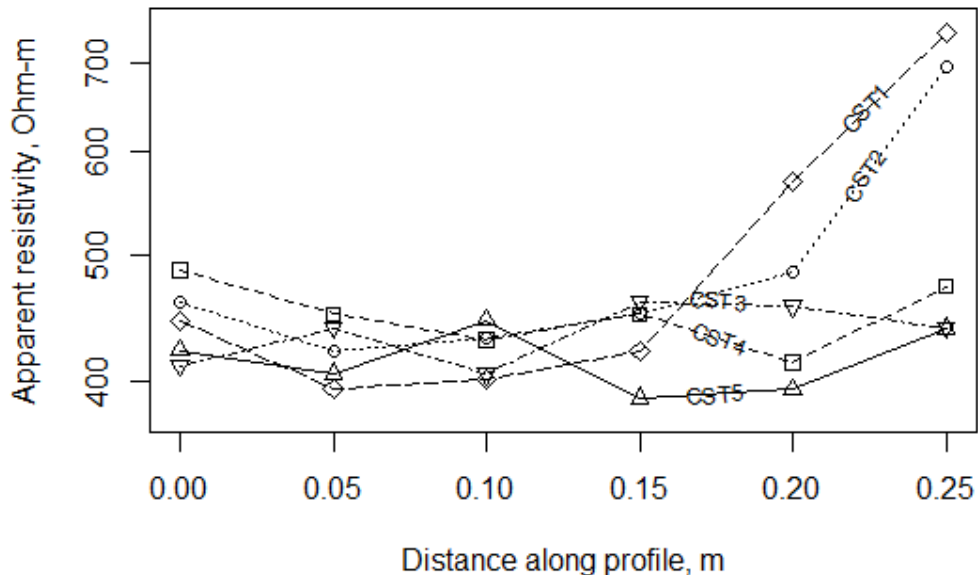


Figure 17. Parallel CSTs of a test bed containing a 10-cm-long artificial void intercepting two profiles at 20 cm

A heat map was then generated to render the spatial variation of apparent resistivity values in two dimensions (figure 18). The coloring of each zone illustrates the apparent value at its center point.

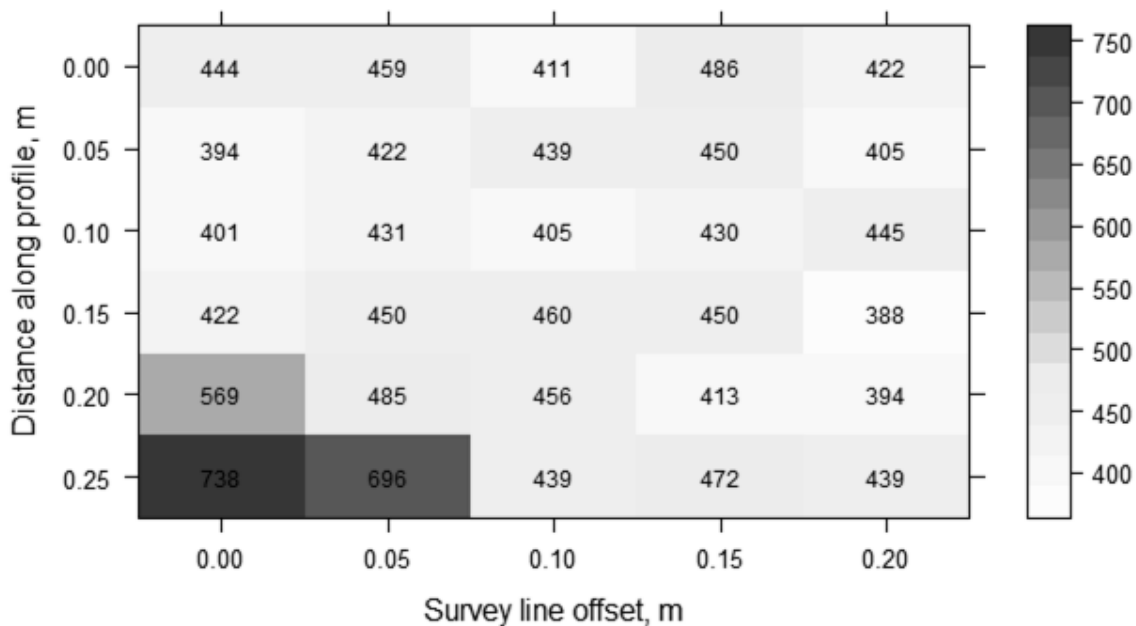


Figure 18. Spatial variation of apparent resistivity (Ohm-m) coinciding with the location of the artificial void in the test bed

The effectiveness of this representation relied on the strong contrast caused by the large variation in values and the close spacing between each data point. The heat map of a terrain that is not affected by a disruptive feature at the depth of interest may display nothing more than the different levels of noise in the measurements.

Therefore, in the analysis of a matrix of CST, it may be useful to concentrate on a study of the fit and the presence of residuals. To this end, a robust analysis in the form of a median polish was performed on the dataset. 433 Ohm-m was identified as the overall median fit of the resistivity 7.5cm below the surface. The row effect was comprised between -25 and 25 Ohm-m and the column effect was found to be relatively similar, varying between -16.5 and 23 Ohm-m. The values for most residuals fell between -67 and 54 Ohm-m. Three data points did not agree with this additively-fit model and showed relatively greater residuals (i.e. 111, 218, and 282). To visualize any clustering and consider spatial variations on a properly weighted scale, a bubble chart was drawn proportionally to the square root of the absolute value of the residuals. The latter correctly highlighted the three data points whose electrode array laid directly on top of the void.

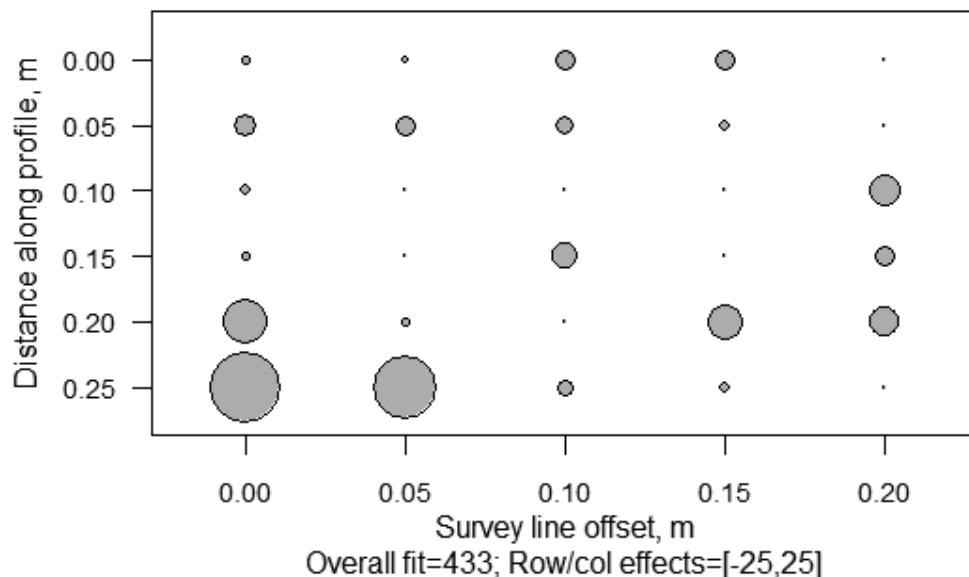


Figure 19. Robust modeling by median polish of the spatial variation of apparent resistivity (Ohm-m). Disks' radius are proportional to the square root of the residuals

6. LIMITATIONS

Earth resistivity readings stand as a proxy for the physical variability of soils (Samouelian, et al. 2004). This makes ER methods an attractive tool, capable of investigating the subsoil and detecting buried features without any digging. Concurrently, it opens ER results to numerous interpretations as resistivity values are the product of a combination of physical properties. For instance, two soil specimens sharing in common the grain size can produce drastically different electrical responses based on their respective moisture content. In addition, the typical range of electrical resistivity for a given sediment tend to overlap with other minerals. Consequently, a fair knowledge of the potential geology at the site is often required to permit the interpretation of ER surveys.

The interpretation method described in Section 4.1 did not rely on an inversion of the readings collected. Instead, apparent resistivity values were considered to assess the variability below the surface of the test beds. The values of apparent resistivity served as a diagnostic of the underground composition. In reality, apparent and true resistivity values are only equal in the case of homogeneous grounds (Telford, Geldart and Sheriff 1990). Another assumption was made in that the vertical variations in resistivity values found in VES surveys (in Section 5.1) were governed by the occurrence of horizontally stratified layers. Similarly, the lateral variations sensed during CST surveys (in Section 5.2) were straightforwardly linked to the detection of a vertical feature. In fact, soil properties vary in all directions and the interpretations based on the one-dimensional sounding and/or profiling of the earth are limited and intricate.

Two- and three-dimensional tomography techniques that implement large grids of electrodes enable the better understanding of complex terrains. However, the black box nature of such a device was recognized to be an issue and encouraged the making of an affordable ER meter that is easy to assemble and intuitive to operate. The device consists of a four-electrode resistivity system that uses conventional electrode measurement sequences such as Wenner and dipole-dipole arrays. The implementation of the latter proved to be unsuccessful due to the unnoticeable values of potential induced by the current dipole. Others previously reported on the low signal to noise ratio characteristic of the dipole-dipole array (Cardimona, 2002; Zhou, Beck and Adams, 2002; Samouelian, et

al., 2004). The use of a Wenner array produced reasonable findings (sections 5.1-2). However, the values of current measured in both setups were low (i.e. in the range of milliAmpere) and clearly suggested the implementation of a greater power supply to best fit the needs of future projects. In contrast with tabletop test beds on the scale of decimeters, previous karst studies have extended at times on the order of kilometers (Mitrofan, Povara and Mafteiu, 2008; Nassimi and Mohammadi, 2016). In order to perform investigation of that extent, one should use a stronger power supply and take the necessary steps to prevent the hazard of electric shocks. Other issues that may arise from the use of higher voltages are the polarization of the ground and a potential switch to AC (Cardimona, 2002; Mikailu, et al., 2015).

For the scope of this work, the calibration of the current sensor was set over the range of $\pm 400\text{mA}$ at 16V. Future undertakings may likely exceed those specifications. Therefore, further developments may include the upgrade to an IC capable of sensing the range of values being studied and, through the use of additional instrument amplifiers, adjusting the maximum resolution over the range of interest. Moreover, the experimental nature of this prototype justified the use of “plug-and-play” breadboards and jumper wires. But the sturdiness and reliability of such connectors may become questionable in field studies of larger scale. Therefore, a switch to shields and soldered connections is highly recommended in the implementation of a semi-permanent device fit for future explorations.

7. CONCLUSION

This study resulted in the implementation of an *affordable* and *easy-to-use* ER meter, which addressed the issues of both the cost and the possible black box nature of laboratory equipment. During confirmatory testing, the prototype showed a satisfactory level of accuracy and precision over a wide range of answers. In the scope of this study, two experiments were conducted in a tabletop laboratory setting to ensure the proper functioning of the proposed device and its overall potential to assess karst-prone sites.

The first one served to evaluate the accuracy of the information provided by the depth sounding of soil layers characteristic of karst terrains. The experiment showed that the low-cost ER meter successfully sensed variations in soil covers, correctly assessed the depth to bedrock, and produced reasonable and repeatable apparent resistivity values.

The second test was intended to study the ability of the device to detect the presence of an artificial air-filled void. The results showed the clear disruptions in apparent resistivity values caused by the vertical feature along a horizontal profile.

In both VES and CST configurations, the use of a Wenner array proved to produce meaningful results that agreed with the specifications of the test beds. However, further testing should explore the implementation and performance of other conventional arrays.

The current work also found that the reliability of the device became limited when it was exposed to relatively low values of current. This finding highlighted the importance of the voltage delivered by the power supply to the system and suggested the potential switch to relatively higher voltages and alternating currents in order to permit the future field investigation of larger sites and deep karst features.

Overall, the proposed device proved to be affordable, intuitive to use, and capable of detecting soil layers and anomalies that are characteristic of karst system exploration.

REFERENCES

- Badmus, B. S., and A. O. Kilasho. 2013. "Fabrication of Electrical Resistivity Equipment and Some Model Studies within Complex Basement Terrain of Southwestern Nigeria." *Research Journal of Physics*.
- Beck, Robert. 1997. "Earth Resistivity Meter." *Everyday Practical Electronics* (Wimborne Publishing, Ltd.).
- Becker, John. 2003. "Earth Resistivity Logger." *Everyday Practical Electronics: Constructional Project*.
- Brinkmann, R., M. Parise, and D. Dye. 2007. "Sinkhole distribution in a rapidly developing urban environment: Hillsborough County, Tampa Bay area, Florida." *Engineering Geology* 169-184.
- Cardimona, Steve. 2002. *Electrical resistivity techniques for subsurface investigation*. Department of Geophysics, university of Missouri Rolla-Mo.
- Carriere, Simon D., Konstantinos Chalikakis, Guy Senechal, Charles Danquigny, and Christophe Emblanch. 2013. "Combining electrical resistivity tomography and ground penetrating radar to study geological structuring of karst unsaturated zone." *Journal of Applied Physics* 31-41.
- Chalikakis, K., V. Plagnes, R. Guerin, R. Valois, and F. P. Bosch. 2011. "Contribution of geophysical methods to karst-system exploration: an overview." *Hydrogeology Journal* 1169-1180.
- Culshaw, M. G., and A. C. Waltham. 1987. "Natural and artificial cavities as ground engineering hazards." *Quarterly Journal of Engineering Geology and Hydrogeology* 139-150.
- Farooq, Muhammad, Samgyu Park, Young Soo Song, Jung Ho Kim, Mohammad Tariq, and Adepelumi Adekunle Abraham. 2012. "Subsurface cavity detection in a karst environment using electrical resistivity (er): a case study from yongweol-ri, South Korea." *Earth Sciences Research Journal* 75-82.
- Florida Senate Interim Report 104. 2011. "Issues relating to sinkhole insurance."
- Ford, D. C., and P. W. Williams. 1989. *Karst Geomorphology and Hydrology*. Winchester, MA: Unwin Hyman Inc.
- Gambetta, M., E. Armadillo, C. Carmisciano, P. Stefanelli, L. Cocchi, and F. Totini. 2011. "Determining geophysical properties of a near-surface cave through integrated microgravity vertical gradient and electrical resistivity tomography measurements." *Journal of Caves and Karst Studies* 11-15.

- Gutierrez, F., M. Parise, J. De Waele, and H. Jourde. 2014. "A review on natural and human-induced geohazards and impacts on karst." *Earth Science Reviews* 61-88.
- Hallof, Philip George. 1957. *On the interpretation of resistivity and induced polarization field measurements*. Dissertation, Massachusetts Institute of Technology.
- Herman, Rhett. 2001. "An introduction to electrical resistivity in geophysics." *American Journal of Physics* 69: 943-952.
- Hiltunen, D. R., and M. Roth. 2003. "Investigation of bridge foundation sites in karst terrane via multi-electrode electrical resistivity."
- Jardani, A., A. Revil, F. Santos, C. Fauchard, and J. Dupont. 2007. "Detection of preferential infiltration pathways in sinkholes using joint inversion of self-potential and EM-34 conductivity data." *Geophysical Prospecting* 749-760.
- Jennings, J. N. 1985. *Karst Geomorphology*. New York, NY: Oxford University Press.
- Juhari, Nabilah Khairunnisa, Nurunadiah Mohd Noor, Mohamad Huzaimy Jusoh, Mohamad Fahmi Hussin, and Ahmad Asari Sulaiman. 2017. "The development of a small range soil electrical resistivity meter based on wenner configuration." *International Journal of Simulation: Systems, Science and Technology*.
- Kaufmann, O., J. Deceuster, and Y. Quinif. 2012. "An electrical resistivity imaging-based strategy to enable site-scale planning over covered paleokarst features in the Tournaisis area (Belgium)." *Engineering Geology* 49-65.
- Kruse, S., M. Grasmueck, M. Weiss, and D. Viggiano. 2006. "Sinkhole structure imaging in covered karst terrain." *Geophysical Research Letters*.
- Land, Lewis. 2012. "Geophysical prospecting for new cave passages: Fort Stanton Cave, New Mexico, USA." *Carbonates and Evaporites* 97-102.
- Mikailu, A., I Abdullahi, M. G. Sani, and S. Huhammad. 2015. "Development of digital resistivity meter." *Advances in Physics Theories and Applications*.
- Mitrofan, Horia, Ioan Povara, and Mihai Maftciu. 2008. "Goelectrical investigations by means of resistivity methods in karst areas in Romania." *Environmental Geology* 405-413.
- Nassimi, Alireza, and Zargham Mohammadi. 2016. "Comparison of the results of pumping and tracer tests in a karst terrain." *Journal of Cave and Karst Studies* 110-118.
- Newton, John G. 1987. *Development of sinkholes resulting from man's activities in the Eastern United States*. U.S. Geological Survey.

- Nordiana, M. M., Rosli Saad, M. N. Nawawi, I. N. Azwin, and Edy Tonnizam Mohamad. 2013. "Case study: shallow subsurface geology mapping using 2-D resistivity imaging with EHR technique." *International Conference on Environmental Science and Development* 134-140.
- Nyquist, Jonathan E., John S. Peake, and Mary J.S. Roth. 2007. "Comparison of an optimized resistivity array with dipole-dipole soundings in karst terrain." *Geophysics* 139-144.
- Park, G., S. Park, M.-J. Yi, H. Rim, S.-J. Cho, and J.-H. Kim. 2010. "Geostatistical integration using 2-D electrical resistivity and 3-D gravity methods for detecting cavities in a karst area." *Environmental Earth Science* 965-974.
- Quinlan, J., and R. Ewers. 1985. "Ground water flow in limestone terrains." *National Symposium and Exposition on Aquifer Restoration and Ground Water Monitoring* 197-234.
- Reynolds, John M. 1997. *An introduction to applied and environmental geophysics*. Cambridge University Press.
- Roth, M., and J. Nyquist. 2003. "evaluation of multi-electrode earth resistivity testing in karst." *Geotechnical Testing Journal* 167-178.
- Samouelian, A., I. Cousin, A. Tabbagh, A. Bruand, and G. Richard. 2004. "Electrical resistivity survey in soil science: a review." *Soil and Tillage Research* 173-193.
- Sharma, Prem V. 1997. *Environmental and engineering geophysics*. Cambridge University Press.
- Sowers, George F. 1996. *Building on Sinkholes: Design and Construction of Foundations in Karst Terrain*. American Society of Civil Engineers.
- Stanley, John. 1981. "Earth Resistivity Meter." *Electronics Today International: How to build gold and treasure detectors*.
- Telford, William Murray, L. P. Geldart, and R. E. Sheriff. 1990. *Applied geophysics*. 2nd. Cambridge University Press.
- Tran, K. T., M. McVay, M. Faraone, and D. Horhota. 2013. "Sinkhole detection using 2D full seismic waveform tomography." *Geophysics* 175-183.
- Trudgill, Stephen Thomas. 1985. *Limestone Geomorphology*. Longman.
- Veni, George, Harvey DuChene, Nicholas C. Crawford, Christopher G. Groves, George N. Huppert, Ernst H. Kastning, Rick Olson, and Betty J. Wheeler. 2001. *Living with karst: a fragile foundation*. American Geological Institute.
- White, William B. 1988. *Geomorphology and Hydrology of Karst Terrains*. New York, NY: Oxford University Press.

- Yang, Xianjin, and Mats Lagmanson. 2006. "Comparison of 2d and 3d electrical resistivity imaging methods." *Symposium on the Application of Geophysics to Engineering and Environmental Problems* 585-594.
- Zhou, Wanfang, Barry F. Beck, and Angela L. Adams. 2002. "Effective electrode array in mapping karst hazards in electrical resistivity tomography." *Environmental Geology* 922-928.
- Zhou, Wanfang, Barry F. Beck, and J.B. Stephenson. 2000. "Reliability of dipole-dipole electrical resistivity tomography for defining depth to bedrock in covered karst terranes." *Environmental Geology* 760-766.
- Zhu, Junfeng, James C. Currens, and James S. Dinger. 2011. "Challenges of using electrical resistivity method to locate karst conduits: a field case in the inner bluegrass region, Kentucky." *Journal of Applied Geophysics* 523-530.

APPENDIX

The code written on the IDE and uploaded to the Arduino board is given below:

```
//Include libraries
#include <Wire.h>
#include <Adafruit_INA219.h>
#include <LiquidCrystal_I2C.h>
#include <SD.h>

// INA219 Sensor and LCD screen attached to I2C (Inter-Integrated Circuit) bus as follows:
// SDA (Serial Data Line) - pin A4 (pink)
// SCL (Serial Clock Line) - pin A5 (white)

// Set the I2C address for each device
Adafruit_INA219 ina219;
LiquidCrystal_I2C lcd(0x27, 2, 1, 0, 4, 5, 6, 7, 3, POSITIVE);

// SD card attached to SPI (Serial Peripheral Interface) bus as follows:
// MOSI (Master Out Slave In) - pin 11 (yellow)
// MISO (Master In Slave Out) - pin 12 (green)
// SLK (Serial Clock) - pin 13 (orange)
// CS (Chip Select) - pin 10 (blue)
const int DefaultCS = 10; // Default output

// Set adequate length for string transfer to SD card
char buffer [10];
// Initialize reading sequence
int id = 1;

//-----
// SETUP SETUP SETUP SETUP SETUP
//-----

// void setup, to run once:
void setup() {
  // Initialize communication with INA219 sensor
  ina219.begin();
  // Sensor defaults calibration in 32V, 2A range
  // Set a lower 16V, 400mA calibration range to improve precision
  ina219.setCalibration_16V_400mA();

  // Initialize communication with lcd screen
  lcd.begin(20, 4);
  // Print title
  lcd.setCursor(0, 0);
  lcd.print("Resistivity Test");
  // Print author
  lcd.setCursor(0, 1);
  lcd.print(" by BDG @ UVA");
  // Wait
  delay(500);
  // Print Status 1
  lcd.setCursor(0, 2);
  lcd.print("Booting...");
  lcd.setCursor(0, 3);
  // Wait
  delay(500);
}
```

```

// Set default CS pin as output
pinMode(DefaultCS, OUTPUT);
// See if SD card is present and can be initialized
if (!SD.begin(DefaultCS)) {
  lcd.print("Card failed"); // Print Error 1
  return; // Exit void setup
}
// See if file can be written/opened
File logFile = SD.open("LOG.csv", FILE_WRITE);
if (logFile) {
  logFile.println(","); // Write a leading blank line
  String header = "I, V, R";
  logFile.println(header); // Write header
  logFile.close(); // and close file
  lcd.print("File initialized..."); // Print Status 2
}
else {
  lcd.print("File failed"); // Else, print Error 2
}
delay(1000);
}

//-----
// LOOP LOOP LOOP LOOP LOOP
//-----

// void loop, to run repeatedly:
void loop() {
  // Clear screen
  lcd.clear();

  // Get current in mA from INA219 sensor
  float current_mA = ina219.getCurrent_mA();
  // Convert to SI unit
  float current = (current_mA / 1000);
  // Print current
  lcd.setCursor(1, 0);
  lcd.print("I= ");
  lcd.print(current_mA,3);
  lcd.print(" mAmps");

  // Arduino senses voltage in 0-5V range
  // A voltage divider creates an output voltage that is a fraction of the input
  float Ra = 1000000; // input resistor value of voltage divider
  float Rb = 100000; // output resistor value of voltage divider
  float RR = (Rb/(Ra+Rb)); // voltage divider ratio
  // Read analog value from sensor A0
  int value0 = analogRead(A0);
  // Calculate voltage sensed at output of voltage divider
  float vraw = (value0*5.0/1024);
  // Adjust voltage at input of voltage divider
  float voltage = (vraw / RR);
  // Print voltage
  lcd.setCursor(1, 1);
  lcd.print("V= ");
  lcd.print(voltage,3);
  lcd.print(" Volts");
}

```

```
// Calculate resistance based on Ohm's law
float resistance = (voltage / current);
// Print resistance
lcd.setCursor(1, 2);
lcd.print("Ra= ");
lcd.print(resistance,1);
lcd.print(" Ohms");
lcd.setCursor(1, 3);

// Compile current, voltage, and resistance data into a string
String dataString = String(dtostrf(current,8,4,buffer)) + "," + dtostrf(voltage,8,6,buffer) +
"," + dtostrf(resistance,8,4,buffer);
//See if file can be written/opened
File logFile = SD.open("LOG.csv", FILE_WRITE);
if (logFile) {
  logFile.println(dataString); // Write string
  logFile.close(); // and close file
  lcd.print("[SD=On, #Rdgs="); // Print Status 3
  lcd.print(id);
  lcd.print("]");
}
else {
  lcd.print("[SD=Off]"); // Else, print Error 3
}
id++;
delay(200); // Time interval between consecutive loops
}
```